Theoretical and experimental study of the unoccupied electronic band structure of Ru(001) by electron reflection

M. Lindroos,* H. Pfnür, and D. Menzel
Fakultät für Physik, Institut für Festkörperphysik E20, Technische Universität München, D-8046 Garching bei München, Federal Republic of Germany
(Received 27 December 1985)

Very-low-energy electron diffraction (VLEED) is used to study the unoccupied electronic states of Ru(001). Experimental and theoretical data are presented for reflection of electrons with energies of the specular beam between 7 and 32 eV and at different angles of incidence between 3° and 28° in both the $\bar{\Gamma}\bar{K}$ and $\bar{\Gamma}\bar{M}$ directions. Two sharp reflection minima at kinetic energies of 11.1 and 12.3 eV (relative to the vacuum level) corresponding to a final-state peak in Ru(001) angle-resolved photoemission and secondary-electron emission are observed near normal incidence. Theoretical VLEED intensity and band-structure calculations are carried out to confirm the origin of the experimental spectral features. An energy-dependent optical potential is shown to be sufficient to explain the observed narrow spectral structures. The observed minima can be reproduced excellently with the imaginary part of the optical potential equal to -0.6 eV at 11 eV above the vacuum level. The minimum at 12.3 eV can clearly be correlated with a high density of states in the *volume* band structure, whereas the other one is assigned to a Shockley-type surface state. The effects of several other parameters on the theoretical spectra are discussed.

I. INTRODUCTION

The band structure of occupied electronic states can be studied by methods like angle-resolved photoemission spectroscopy (PES) or the de Haas–van Alphen effect. These experimental results are well understood within the frame of various theoretical approaches.[1] For the unoccupied states above the Fermi level, methods such as inverse photoemission or x-ray-absorption near-edge structure (XANES) have been established more recently. Information about the band structure above the *vacuum* level, however, cannot only be gained by these methods, but also by secondary electron emission (SEE),[2] excited either by primary electrons or photons, and by low-energy electron diffraction (LEED) at very low energies (VLEED).[3] As in VLEED, electronic states are, in principle, resonantly occupied in precisely defined directions, a signal-to-background ratio much higher than with other methods and a more precise determination of the dispersion can be expected. *Minima* in VLEED should occur where the high bulk density of states couples well to free-electron-like states so that the probability of being reflected back is small because the electron can travel far into the crystal. In a band gap, however, the electron cannot penetrate into the crystal. The result is *high* reflectivity.

One of the motives for starting this work was the observation of a strong final-state peak in PES and SEE (Refs. 4 and 5) in Ru(001), at a kinetic energy of 16.5 eV relative to E_F, which has been explained by a high final-state density deriving mainly from the empty $4f$ bands.[4] If this interpretation is correct, then the VLEED IV spectra should show a minimum at the same energy, as the final state in photoemission is a time-reversed LEED state. Thus, the essential origin of the final-state peak in photoemission is the same as that of VLEED structures, although there are differences in detail. It will be shown that such a structure is indeed observed. In the present study we have measured specular VLEED IV curves of Ru(001) in the energy range from 7 up to 32 eV. Energies are defined with respect to the vacuum level. The angle of incidence has been varied between 3° and 28° in both $\bar{\Gamma}\bar{K}$ and $\bar{\Gamma}\bar{M}$ directions. Our main interest will focus on two rather narrow minima at energies of 11.1 and 12.3 eV and a small peak at 11.9 eV between these minima. Similar spectral features in specular electron diffraction have been reported earlier, e.g., for Cu(111), Cu(001), Ni(111), CdS(0001),[6] for Au(111), Ag(111), Pd(111), Cu(111), Ni(111), Al(111),[3] and for Ni(001).[7] VLEED of Ru(001) differs from the previous studies by spectra having very sharp spectral structures.

Theoretical reproduction of the dip at the energy of 22.5 eV in Cu(111), similar to the minima in Ru(001), has been further studied by Lindgren *et al.*[8] and Le Bosse *et al.*[9] Lindgren *et al.*[8] explain the origin of the dip by a variation of the electron absorption inside and outside muffin tins of the crystal potential. Le Bosse *et al.*[9] reproduce the dip by allowing an imaginary part of the optical potential (denoted here as V_{PI}) to depend on two-dimensional reciprocal-lattice vectors, **g**. In reality, the optical potential depends on energy, space, and momentum. The derivation of this exact dependence is a tremendous task and so in most calculations this energy, space, and momentum-dependent optical potential has been simply replaced by a constant. The results of LEED or PES calculations with constant V_{PI} have yielded such good results that this crude approximation has been tolerated. When in spectra, there are some, usually subtle, features which cannot be explained with constant V_{PI}, a more complicated approximation has to be used.[8,9] We let our optical potential depend on electron energy as did

Lindgren *et al.*[8] Since this energy dependence is not exactly known, we have used the jellium model as approximated by Hedin and Lundqvist[10] to obtain a functional shape of the optical potential. In our case, it turns out that it is not necessary to make V_{PI} space dependent in the bulk, but by proper scaling of V_{PI} below and above the plasmon cutoff energy we can excellently reproduce the experimental spectra.

We will also show how the spatial variations of the surface barrier are included in the VLEED calculations and we will discuss briefly the influence of the z dependence of the surface barrier on IV curves.

First, we will briefly describe our experimental system and show typical results. Then we will present a short outline of the theory behind our calculations and discuss properties of the optical potential. Finally, we will present detailed experimental results and compare them with theory.

II. EXPERIMENTAL AND TYPICAL RESULTS

For these measurements, standard four-grid LEED optics were used and the intensity of the (00) beam was recorded with a highly sensitive spot photometer. The angle of aperture of about 3° guarantees that the total (00) beam intensity is collected even at the lowest possible energies (7 eV), where the primary beam is no longer well focused. In order to make work at such small energies possible, a double mu-Metal shield around the chamber reduces the magnetic field between sample and the LEED screen to less than 10 mG. The primary beam current for all measurements was 5 nA, which was stabilized to $\approx \pm 2\%$. By alternately switching the (dc) heating current of the sample and the electron beam using an additional voltage of -180 V at the Wehnelt cylinder, the sample could be set to any desired temperature during measurements. Measurements shown here, however, were recorded at 90 K. The sample was cut by spark erosion, oriented by Laue diffraction to better than 0.25°, and polished with diamond pastes down to 0.25-μm grain size. *In situ* cleaning was done by heating-cooling cycles in 1×10^{-6} Torr O_2, as described elsewhere.[11] The cleanliness was checked by Auger-electron spectroscopy (AES) and $\Delta\Phi$ measurement during adsorption and desorption of H_2.[12]

Some typical results are shown in Fig. 1. A strong double minimum in reflection is seen to occur at 11.1 and 12.3 eV above E_v. We have included a typical curve of photoelectron emission with photon energy of ≈ 38 eV for which the final-state peak does not interfere with emission from valence bands. It is obvious that the structures in VLEED and SEE coincide, but that the former are much sharper and better resolved. The small but clearly observable differences will be discussed in a subsequent paper,[13] in which we will attempt to simulate the secondary emission spectra in photoemission. Nevertheless, the correlation is obvious. In the following, we will concentrate on the explanation of the VLEED spectra and their connection to the unoccupied band structure and the reflection process.

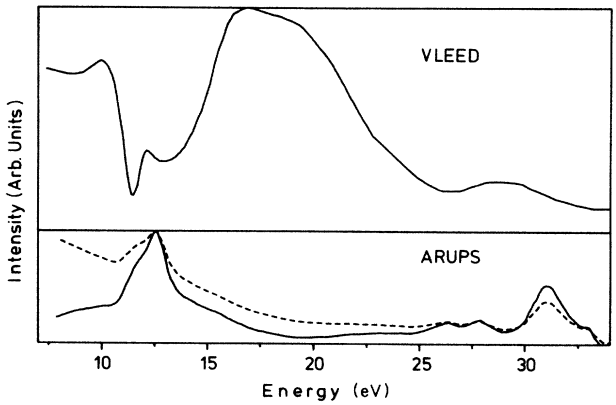

FIG. 1. (a) Experimental VLEED IV curve near normal incidence (3° off normal). (b) For comparison secondary-electron spectrum excited by photons of 38 eV at normal emission of Ru(001) (Refs. 4(b) and 5), illustrating the correspondence between the SEE peak around 11 eV and the LEED minima at the same kinetic energy. From the original photoemission spectrum (dashed line) a smooth background was subtracted.

III. THEORY

In this section, we will first show the theoretical connection between LEED and photoemission intensities. Starting from a general equation for the photoemission current, a time-reversed LEED contribution is isolated. This will show that the same spectral variations, which are present in LEED spectra, are also present in photoemission spectra; but, of course, they might be strongly modified or suppressed by other contributions to the photoemission process. According to Pendry,[14] the photocurrent in the photoemission process can be derived from

$$I(k_{||},E)=\frac{-1}{\pi}\mathrm{Im}\langle k_{||}\,|\,G_2^{+}\Delta G_1^{+}\Delta^{\dagger}G_2^{-}\,|\,k_{||}\rangle\ . \tag{1}$$

In this equation, G_1^{+} and $G_2^{\pm}$ describe the propagation of the hole and the electron state, respectively, in the crystal. Δ and $\Delta^{\dagger}$ describe the creation and annihilation of an electron-hole pair in the crystal by the photon field. Atomic units, Hartrees, and Bohr radii are used in all equations, unless otherwise stated. $k_{||}$ is the parallel component of the momentum of the incoming and outgoing electron,

$$k_{||}=\frac{1}{a}E_k^{1/2}\sin\Theta\ , \tag{2}$$

a is the Bohr radius, E_k the electron energy (with respect to the vacuum level), and Θ is the emission angle.

The final state of the electron in the photoemission process is a time-reversed LEED *state*, Φ_2^{*}, as was originally demonstrated by Adawi.[15] Φ_2^{*} is defined by

$$\Phi_2(\mathbf{r}')^{*}=\langle\mathbf{r}'\,|\,G_2^{-}\,|\,k_{||}\rangle\ . \tag{3}$$

In the computer program for photoemission,[16] Φ_2 is calculated in a plane-wave representation, valid between the $(j-1)$th and jth atomic layers, called $\Phi_{2,j}$ in the following. The crystal potential, which has the muffin-tin form,

is constant outside the muffin-tin radius, and the electron wave function can be expressed as

$$\Phi_{2,j}(\mathbf{r})=\sum_{\mathbf{g}} a_{j\mathbf{g}}^{+}\exp[i\mathbf{k}_{\mathbf{g}}^{+}\cdot(\mathbf{r}-\mathbf{c}_j)] + a_{j-1\mathbf{g}}^{-}\exp[i\mathbf{k}_{\mathbf{g}}\cdot(\mathbf{r}-\mathbf{c}_{j-1})] . \quad (4)$$

$a_{j\mathbf{g}}^{\pm}$ are wave amplitudes and $\mathbf{c}_j$ is the origin of the jth layer, and the V_{PI}-dependent wave vector, $\mathbf{k}_{\mathbf{g}}^{\pm}$, is defined by

$$\mathbf{k}_{\mathbf{g}}^{\pm}=\{\mathbf{k}_{||}+\mathbf{g},\pm[2(E_k+V_r-iV_{PI})-|\mathbf{k}_{||}+\mathbf{g}|^2]^{1/2}\} , \quad (5)$$

where V_{PI} is the imaginary part and V_r the real part of the optical potential. From Eq. (4) we notice that the intensity of the diffracted specular beam in VLEED will be

$$I_{00}=|a_{0,00}^{-}|^2 . \quad (6)$$

Theoretical calculation of the diffracted current, I_{00}, where 00 refers to the specular beam, is a normal problem of LEED.[17,18] However, in the present case we have two special conditions to take into account. First, our energy values from 7 up to 32 eV are smaller than in an ordinary LEED study. Secondly, it turns out that in order to produce the correct width of the spectral structures around 11 eV in our theoretical spectra, we have to use an imaginary part of the optical potential six times smaller than in ordinary LEED studies. Both conditions lead to considerably increased convergence problems.

We have taken the final-state part of the angle-resolved photoemission program originally developed by Hopkinson *et al.*[16] to calculate I_{00} of Eq. (6). That computer program was further expanded by Larsson[19] to include two atoms and several layers in the unit cell. We need this extended version for hexagonal Ru(001), which has two atoms (atomic layers) per unit cell.

The advantage of the use of the photoemission-based programs (which probably were originally derived from LEED programs) is that the convergences of the calculations are more certain than in ordinary LEED programs designed for higher energies with larger V_{PI}. The better convergence is mainly due to the calculation of the multiple scattering *within* an atomic layer. In the photoemission program, this part is carried out using Kambe's[20] method, whereas in LEED programs, time-saving direct summation methods are usually used;[17] the latter, however, do cause problems with convergence in the present case. A further advantage is that it is possible to use these same programs to study the photoemission of the above-mentioned final-state peak.[13]

This study clearly demonstrates the necessity to use an energy-dependent imaginary part of the optical potential in VLEED intensity calculations. To show how this quantity is included in calculations we will derive some central quantities of LEED intensity calculations. Amplitudes of the diffracted electrons in Eq. (6), $a_{0\mathbf{g}}^{-}$, are calculated through the following equation:

$$a_{0\mathbf{g}}^{-}=\sum_{\mathbf{g}'} P_{S\mathbf{g}}^{-}M_{\mathbf{g}\mathbf{g}'}^{-+}P_{S\mathbf{g}'}^{+}a_{0\mathbf{g}'}^{+} , \quad (7)$$

where the amplitude of the incident electron, $a_{0\mathbf{g}}^{+}$, is given by

$$a_{0\mathbf{g}}^{+}=\frac{-i}{k_{\mathbf{g}_z}^{+}}\delta_{\mathbf{g},00} . \quad (8)$$

$P_{s\bar{0}0}^{\pm}$ are propagators from the surface barrier to the first atomic layer. In general, matrices

$$P_{\mathbf{g}\mathbf{g}'}^{\pm}=e^{(\pm i\mathbf{k}_{\mathbf{g}}\cdot\mathbf{d})}\delta_{\mathbf{g}\mathbf{g}'} \quad (9)$$

represent the propagation factors, which account for phase change and attenuation ($\mathbf{k}_{\mathbf{g}}$ is complex due to V_{PI}) between atomic layers. $\mathbf{d}$ is the distance between two adjacent atomic layers, $\mathbf{c}_j-\mathbf{c}_{j-1}$. In Eq. (7), $M_{\mathbf{g}\mathbf{g}'}^{-+}$ is the total reflection matrix (bulk and surface combined), describing the distribution of the amplitudes of the electrons diffracted backwards.

We calculate the total reflection matrix using the standard layer doubling[17] method. The use of this time-consuming method is once again necessary to secure convergence of the calculations. One of the relevant equations of M^{+-}, M^{-+}, M^{--}, or M^{++} for the doubling is

$$M^{-+}=R_a^{-+}+T_a^{--}(I-P^{-}R_b^{-+}P^{+}R_a^{+-})^{-1}\times P^{-}R_b^{-+}P^{+}T_a^{++} , \quad (10)$$

where subscripts a and b refer to first and second layers to be combined. These doublings are repeated until the values of the elements in M^{-+} no longer change within the accepted accuracy (i.e., $M^{-+}=R_a^{-+}$). In practice, this method converges very fast (3 or 4 doublings), but convergence depends on the magnitude of V_{PI} (improving with increasing $|V_{PI}|$).

Reflection and transmission matrices of one atomic layer, R and T, respectively, in Eq. (10) are calculated according to

$$T^{++}=I+Q^{++} , \quad (11)$$

$$R^{-+}=Q^{-+} . \quad (12)$$

$Q_{\mathbf{g}\mathbf{g}'}^{-+}$ is defined by

$$Q_{\mathbf{g}\mathbf{g}'}^{-+}=\sum_{\substack{l',m',\\ l,m}}\frac{i8\pi^2}{\kappa\Omega k_{\mathbf{g}z}^{+}}i^{l}(-1)^{m}Y_{l',-m'}(\hat{\mathbf{k}}_{\mathbf{g}'}^{+})\times[1-X(\kappa_{\mathbf{g}}^{\pm})]_{l'm'lm}^{-1}\times i^{-1}Y_{lm}(\hat{\mathbf{k}}_{\mathbf{g}}^{-})e^{(i\delta_l)}\sin(\delta_l) , \quad (13)$$

where $\kappa=(2E)^{1/2}$ and Ω is the area of the unit cell. δ_l are l-wave phase shifts due to the crystal potential. Y_{lm} are spherical harmonics. X is the $\mathbf{k}_{\mathbf{g}}$-dependent matrix, taking care of multiple scattering within the atomic layer.

As an input crystal potential, the tabulated self-consistent potential of Moruzzi *et al.*[21] was used. At these small energies, 13 two-dimensional reciprocal-lattice vectors and four phase shifts were sufficient.

IV. SURFACE BARRIER AND OPTICAL POTENTIAL

In the original photoemission program, as well as in LEED programs, the spatial shape of the surface barrier is usually described by a step function. The height of the potential is then taken equal to the real part of the optical potential. The spatial position of the step is usually taken as one-half of the distance between atomic layers outside the outermost atomic layer.[17,18] V_{PI} defines the height of the imaginary surface barrier. The detailed study of the experimental and theoretical spectra will show that spatial properties of the surface barrier have some minor influence in achieving good agreement between theory and experiment. The main factor, however, is the energy dependence of the height of the imaginary surface barrier, V_{PI}.

The surface described in the simplest case by a step-function-like barrier potential is a source of surface states, and could possibly be responsible for the observed minimum around 11 eV. Once we have a surface barrier, so-called Shockley-type surface states might be present. If we described the z dependence (normal to the surface) by using an image-type potential, we might have so-called image-potential-induced surface states. After specifying a certain z-dependent surface barrier potential, we will show how to include it in our VLEED calculations.[22] We will also briefly describe the procedure used to obtain the energy-dependent shape of our optical potential.

Besides the step-function-like surface barrier, we have also tested another barrier shape, following the formalism developed by Rundgren and Malmström,[23] which has a complicated z dependence. In it, the surface potential is taken to be uniform in the (x,y) plane (parallel to the surface) and to vary in the z direction, as

$$\mathrm{Re}V(z)=\begin{cases}-13.6/2z \text{ eV}, & z<-1.6 \text{ Å}\\ \text{a third-order polynomial}, & -1.6<z<0.0 \text{ Å}\\ V_{r0}, & 0.0 \text{ Å}<z\end{cases} \tag{14}$$

$$\mathrm{Im}V(z)=\begin{cases}(V_{PI})_0/z^2, & z<-2.5 \text{ Å}\\ \text{a third-order polynomial}, & 1.0 \text{ Å}<z<0.0 \text{ Å}\\ V_{PI}, & 0.0 \text{ Å}<z\end{cases} \tag{15}$$

where z is increasing towards the metal. Third-order polynomials join the different pieces of the potential making $V(z)$ and its first derivative continuous. For V_{r0} we have used a value of -14 eV (Ref. 24), for V_{PI}, -2.0 eV, and for $(V_{PI})_0$, zero, in most cases. Using this potential and the computer program of Malmström *et al.*,[23] we have calculated r_S and t_S, the reflection and transmission coefficients for the surface barrier. The values of the parameters in Eqs. (14) and (15) have not been optimized; they just present some reasonable values for the surface barrier. For an exact determination of these parameters, we would need high resolution VLEED data. For simplicity, V_{r0} or V_{PI} in Eqs. (14) and (15) usually are not made energy dependent in our calculations.

The spatial properties of the surface barrier described by the energy-dependent r_S and t_S were connected to VLEED calculations by introducing new surface propagators $P_{S,\text{new}}$ as proposed by Hall *et al.*[22] In order to account for possible multiple scattering between surface barrier and bulk, the new surface propagators are calculated by

$$P^{+}_{S,\text{new}}=(1-P^{+}_{S}r^{+-}P^{-}_{S}M^{-+})^{-1}P^{+}_{S}t^{++}\,, \tag{16}$$

$$P^{-}_{S,\text{new}}=t^{--}P^{-}_{S}(1-M^{-+}P^{+}_{S}r^{+-}P^{-}_{S})^{-1}\,. \tag{17}$$

By replacing the old surface propagators P_S in Eq. (7) with these new ones, the effects of a more realistic surface barrier are included in our VLEED calculations. The widths of the spectral structures around 11 eV are so narrow (see Fig. 1) that V_{PI}, which, in addition to the gaps of the band structure, is responsible for the widths of peaks in this energy range, has to be selected relatively small. As the peaks in experimental spectra at higher energies are much broader, we allowed our V_{PI} to be energy dependent as the simplest approximation. For the energy dependence of V_{PI}, we present in the following, for comparison, two analytical models and one numerical model, which are used in ordinary LEED calculations.

Andersson *et al.*[25] have derived a functional representation of V_{PI} by fitting the experimental widths of the peaks in their IV curves. For nickel, e.g., they have found the following function:

$$V_{o,i}=-1.09-\frac{2.91}{1+\exp[-0.183(E-E_0)]} \text{ eV}\,, \tag{18}$$

where E_0 is taken equal to 35 eV.

Duke *et al.*[26] have introduced the following relation for V_{PI}:

$$V_{o,i}=\frac{\hbar^2}{2m\lambda_{ee}}\left[\frac{2m}{\hbar^2}(E+V_{o,r})\right]^{1/2}\,, \tag{19}$$

where λ_{ee} is the damping length, which might also depend on energy. Some other analytical forms of V_{PI} exist,[27] but these two represent typical energy dependences of V_{PI}.

The energy dependence of the optical potential in the Hedin-Lundqvist jellium theory can be written as[17,28]

$$V_o=V_r+iV_{PI}=Z(k)M(k)+[1-Z(k)]M(k_F)\,, \tag{20}$$

where $M(k,r_s)$ is the electron self-energy and the renormalization constant Z is

$$Z(k,r_s)=\left[1-\frac{\delta M(k,E(k))}{\delta\omega}\right]^{-1}\,. \tag{21}$$

Such a complicated optical potential has been used by, e.g., Neve *et al.*[29] or Lindgren *et al.*[8] The real part of the optical potential was calculated using Eqs. (20) and (21). For the imaginary part, they have used an experimentally adjusted potential whose shape, however, is reminiscent of the shape of the imaginary part of the Hedin-Lundqvist potential.

The important quantity of the above model of $V_{PI}(E)$ is the plasmon cutoff energy. From the shape of the optical potential of Eq. (20), the absolute value of V_{PI} is expected

to be small below this energy and to increase drastically above it. The threshold excitation energy for the plasmon of momentum k_c is[30]

$$\omega_p(k_c)=\omega_p(0)\left\{1+\frac{6E_F^2}{5[\omega_p(0)]^2}\left[\left[1+\frac{\omega_p(0)}{E_F}\right]^{1/2}-1\right]^2\right\}. \tag{22}$$

For Ru,

$$\omega_p(k_c)\approx 1.18\omega_p(0)=11.9\text{ eV},$$

where $\omega_p(0)$ is the plasmon energy with plasmon momentum equal to zero. The theoretical plasmon energy of 11.9 eV has to be compared with the experimental energy loss value of 23.5 eV.[31] This large discrepancy requires rejection of the exact jellium theory, which is not surprising, as Ru cannot be considered to be a good jellium metal. We have therefore derived the shape of our V_{PI} using graphs of M and Z, and proper energy scaling to get $\omega_p\approx 23.5$ eV. The absolute value of $(V_{PI})_{\text{tot}}$, where V_{tot} includes instrumental broadening, was determined from comparison between theoretical and experimental spectra. We define $(V_{PI})_{\text{tot}}$ as

$$(V_{PI})_{\text{tot}}=\{(V_{PI})_0^2+[cV_{PI}(E)]^2\}^{1/2}, \tag{23}$$

where $(V_{PI})_0$ is the contribution from instrumental broadening. Its value and that of parameter c has to be derived from experimental spectra.

The presence of crystal structure means that the wave vector of the plasmon loss is not uniquely defined. In order to take the distribution of the plasmon wave vectors into account, we have used polynomials of third order for V_{PI} in the regions around the cutoff energy instead of a sharp cutoff behavior as given by Eq. (20).

V. RESULTS AND DISCUSSION

A. Connection between *IV* curves and band structure

If the imaginary part of the optical potential, which correctly reproduces experimental spectra, is sufficiently small, it is possible to derive information about the final-state band structure. In particular, it appears feasible to accurately determine energies and k values (Γ or A) of some critical points of the band structure. We first restrict ourselves to (near) normal reflection. In Fig. 2 we demonstrate this direct connection between bulk band structure and theoretical electronic reflectivity for normal reflection. We present a theoretical IV curve of the (00) beam at normal incidence, and the corresponding final-state band structure calculated with a very small and constant V_{PI} equal to -0.0003 eV. The calculation of band structures in our formalism is described in a more detailed way in Ref. 5. Since we use a complex potential, our k values are also complex. When $\text{Im}(k_\perp)$ is allowed to be nonzero, the maximum of one energy band is joined across the band gap by a real energy line to the minimum of a higher band.[32] In Fig. 2 we show, for clarity, only those parts of the joining lines which have $\text{Im}(k_\perp)<0.6$ ΓA instead of all 13 bands available from calculations.

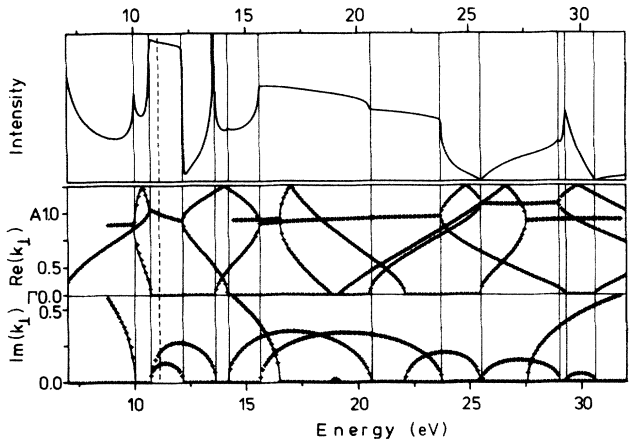

FIG. 2. $I_{00}(E)$ curve at normal incidence and final-state band structure of Ru(001) calculated with V_{PI} equal to -0.0003 eV. Dashed lines show the energy of the empty surface states. Only those bands are shown which have $\text{Im}(k_\perp)<0.6$ ΓA.

In order to obtain converged results for the bulk reflection matrix we had to use 16-layer doublings, which corresponds to penetration of electrons into 65 536 atomic layers. As can be seen in Fig. 2, I_{00} still has no flat-topped peaks, even in the band gaps, as one would expect from a simpler model, or $V_{PI}=0$ calculations.[3] There are two phenomena determining the intensity of the IV curves. Firstly, at electron energies within a band gap, no propagation into the crystal can take place, producing high reflectivity. Secondly, a high one-dimensional density of states produces a small reflectivity. Together, these two effects sometimes dictate the IV intensity in a rather complicated way. This is demonstrated in Fig. 2. There are three features worth mentioning. First, we obtain no extremum behavior at the A point in the Brillouin zone, since $dE/dk_\perp$ is not usually zero at that k point. Secondly, there are some bands which do not show up at all in IV curves for normal incidence. The **G** vector (three-dimensional reciprocal-lattice vector) of the free-electron bands corresponding to these bands is not normal to the surface. Here, we seem to have the same kind of behavior of intensity as in photoemission with Mahan's primary and secondary cones.[33] Furthermore, we point out that the strength of the change in the IV curves when $dE/dk_\perp=0$ seems to depend on whether the corresponding free-electron $E(k)$ point is on or close to the free-electron band with **G** normal to the surface or not.

Thirdly, we have not always a maximum in our reflectivity when $dE/dk_\perp$ is equal to zero. We might also have a minimum, as can be seen at the energies 25.5 or 30.6 eV. A close connection between band structure and reflectivity, or $I_{00}(E)$, is obvious in this extreme theoretical case and the origin of the spectral structures can be explained directly from band structure.

B. Determination of the optimal V_{PI}.

Next, we have determined the value of V_{PI}, which correctly reproduces the minima in the experimental spec-

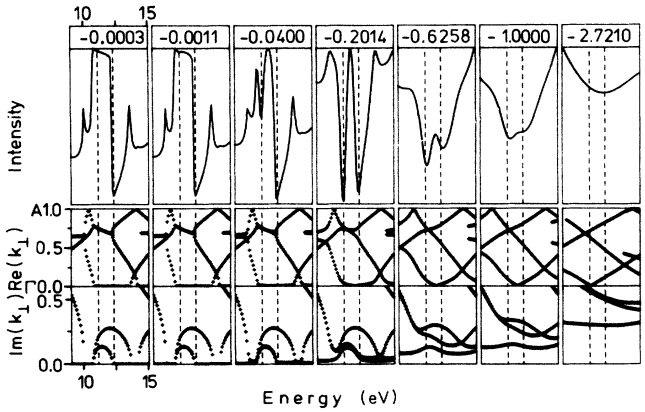

FIG. 3. $I_{00}(E)$ curves and corresponding final-state band structure calculated with various imaginary parts of the optical potential, given in the figure headings. Dashed lines mark the energy positions of the two sharp minima.

trum around 11 eV. In Fig. 3 we show a series of I_{00} spectra calculated with different constant values of V_{PI}. The spatial shape of the surface barrier is taken as a step function.

In the middle and lower frames, $\mathrm{Re}[k_\perp(E)]$ and $\mathrm{Im}[k_\perp(E)]$ are shown. For clarity, all displayed bands and particularly joining lines have $\mathrm{Im}(k_\perp)$ smaller than 0.6. *IV* curves in the topmost frame have a pronounced minimum at 12.3 eV, the energy position of which stays constant at all V_{PI}'s. This minimum is due to the high one-dimensional density of states at the upper edge of the band gap between 10.8 and 12.2 eV. With a small increase in V_{PI}, a second minimum at 11.1 eV *in the band gap* starts to develop. When $V_{PI}=-0.2$ eV, the second minimum is deeper and bigger than the 12.3-eV minimum. This still rather small V_{PI} does smooth other spectral features slightly, but we can still identify the origin of most features. A further increase in V_{PI} only smooths structures more strongly. With a typical LEED value of V_{PI}, -2.7 eV, only a very broad structure around the 12.3 eV minimum is left and the band structure is already rather free-electron-like.

Comparing the shape of the minima in the experimental and theoretical spectra of Fig. 3, we obtain the best agreement with $V_{PI}=-0.625$ eV at 11.5 eV. This value of V_{PI} is the first boundary condition of our semiempirical V_{PI}. Another condition for Eq. (23) comes from the intensity ratios of the maxima at 18 and 28 eV. The optical potential in Eq. (23) fulfills the two boundary conditions with $c=0.5$ and $(V_{PI})_0=-0.544$ eV.

C. The origin of the 11.1-eV minimum

The value of $\mathrm{Im}(k_\perp)$ is a measure of the localization of the band-gap state.[34] From Fig. 3 we achieve for the 11.1-eV minimum, $\mathrm{Im}(k_\perp)=0.13$ in units of ΓA, which leads to a decay distance of 5.2 a.u., corresponding to three atomic layers. By an increase of V_{PI}, scattering contributions from the surface are enhanced relative to the bulk because of the increased damping. This exact behavior is found for the state responsible for the 1.11-eV minimum. So this state must be localized near the surface.

The surface-state interpretation of the 11.1-eV structure is further supported by the observation that the shape of this minimum in *IV* curves (and also in secondary emission) is very sensitive to the presence of adsorbates.[35]

The strong dependence of the 11.1-eV minimum in the *IV* spectra on the value of V_{PI} is a bit surprising. We have written down theoretical quantities of the *IV* calculation to clarify this V_{PI}-dependence in Eqs. (7)—(13). V_{PI} is included in the theory via $k_\perp$ as defined in Eq. (5), so every term that depends on $k_\perp$ can give rise to V_{PI}-dependent spectral features. Such quantities are all propagators as well as the Q matrices, as can been seen from Eqs. (9) and (13). By inspecting individual values of the quantities of Eq. (7) with different V_{PI}'s, we have found that the amplitude of the incident wave, $a^+_{0\mathbf{g}}$, or the propagators $P^\pm_{s\mathbf{g}}$ do not change significantly with V_{PI}. On the other hand, the values of the elements of $M^{-+}_{\mathbf{gg}'}$ seem to be very sensitive to the value of V_{PI}. However, it turns out that all 7×7 complex elements (seven $\mathbf{g}$ vectors as basic vectors are enough to produce these theoretical spectra) of that matrix have the same order of magnitude and thus, e.g., off-diagonal elements cannot be omitted or considered as perturbation in the analysis of the V_{PI} dependence. Any such simplifications, which are usually acceptable in the analysis of the image-type surface-barrier-induced surface states,[36] are not possible here.

A possible explanation for the minimum in the band gap between 10.9 and 12.2 eV is the presence of an unoccupied Shockley-type surface state. As pointed out in our previous photoemission study,[5] the energy position of such a surface state could depend on the spatial position of the surface barrier (at least when a steplike surface barrier is used). However, our test VLEED calculations do not show any changes in the energy positions of the spectral features as a function of the position of the surface barrier, with respect to the first atomic layer. The only noticeable effect is a small attenuation of the oscillations of intensity in the *IV* curve due to the longer traveling path of electrons in the absorbing potential.

One definition of a surface state is that the zero amplitude of the incident wave results in a finite amplitude of reflected waves,[37] and if R is the matrix of reflection coefficients, this means that

$$\det R=\infty\ . \tag{24}$$

In principle, we have defined our R in Eq. (10) and due to symmetry we have $R^{-+}=R^{+-}$. Obviously, Eq. (24) can be fulfilled if

$$\det(\mathbb{1}-P^- R_b^{-+} P^+ R_a^{+-})=0\ . \tag{25}$$

In the case of a steplike surface barrier, we can further approximate $R_a=R_{\mathrm{surface}}=0$, but we still reproduce the minimum around 11 eV. So the minimum is not due to the shape of the surface barrier or the multiple scattering between surface barrier and the first atomic layer. This also explains why the minimum is independent of the position of the surface barrier with respect to the outermost

atomic layer. The 11.1-eV state is *not* localized outside the outermost atomic layer as are, e.g., the image-type surface states.

The next place to look for the surface state would be the region between the first and second atomic layers. We have chosen R_b^{-+} as the bulk reflectivity and R_a^{+-} as the reflectivity of the atomic layer as defined in Eq. (12). In this calculation, V_{PI} was set constant and equal to -0.2 eV, corresponding to the extremal cases of the intensity of the 11.1-eV minimum (see Fig. 3). In Fig. 4, the dashed line and the solid line correspond to *IV* curve and to the absolute value of the determinant in Eq. (25), respectively. Figure 4 clearly demonstrates that the minimum is not exactly due to resonances as defined by Eq. (25), although the value of the determinant varies strongly in the relevant surface-state energy range. We seem to have the same behavior here as with the threshold effects in LEED, namely the oscillations have an interference origin[36] and not a resonance origin as demanded by Eq. (25). On the other hand, we might have some energy shift mechanism of the spectral features due to the complex potential. This effect has been discussed in normal LEED theories, e.g., by Van Hove and Tong.[18] As pointed out before, we cannot represent the reflected intensities in any simple approximative form to study the origin of the 11.1-eV minimum in more detail, because the terms in the reflection matrices are all of the same order of magnitude. So we interpret the origin of the 11.1-eV minimum to be an empty surface-state, which extends some atomic layers from the surface into the bulk. This surface state results from interference of the multiply scattered electron waves between atomic layers.

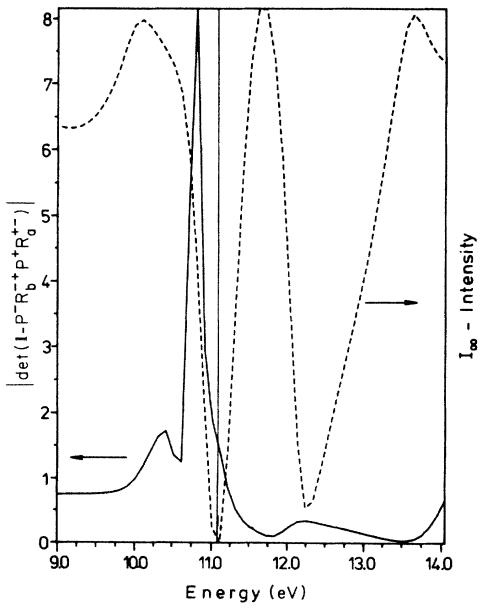

FIG. 4. Part of the theoretical *IV* curves (dashed) and the value of the surface-state determinant (solid) of Eq. (25) showing that the minimum at 11.1 eV does not coincide with the zero of the determinant.

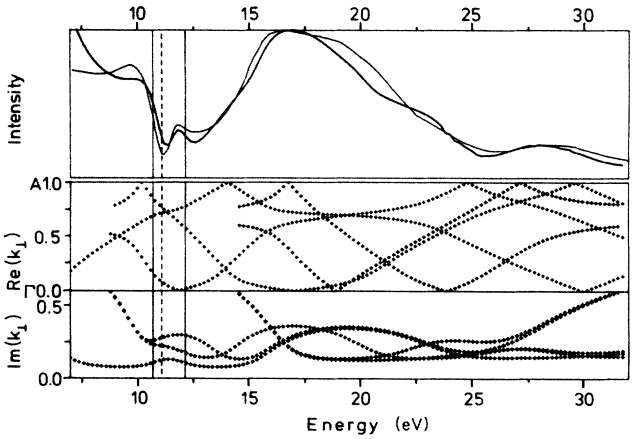

FIG. 5. Experimental (thin line) and optimized theoretical (thick line) $I_{00}(E)$ curves and corresponding final-state band structure. The polar angle of electrons is 3° for *IV* curves and zero for the band structure. See Fig. 2.

D. The optimal *IV* curve, band structure, and optical potential

In Fig. 5 we show experimental and theoretical spectra at the smallest experimentally possible polar angle, 3°, and the corresponding final-state band structure. The theoretical spectrum and the band structure have been calculated using the optimized optical potential derived above. The band structure is calculated for clarity and for the reader's convenience at normal emission, as obvious by the degenerate bands between 17 and 27 eV. Figure 5 displays such good agreement between experimental and theoretical *IV* curves that we are convinced that our theoretical model with energy and z-dependent surface barrier potential is basically correct. Further improvement in agreement could be gained by optimizing various parameters responsible for the shape of the surface barrier in Eqs. (14) and (15). Figure 5 clearly indicates that a derivation of band-structure information from VLEED data is not possible without detailed theoretical support. The presence of the surface-state-induced structures, already rather smoothed spectra and the complex bands hinder direct determination of the $E(k)$ points. Notice particularly that our experimentally observable extrema do not fall on the Brillouin zone boundary in Γ (or A) points, i.e., corresponding arguments for the determination of the high symmetry lines of structures should be taken with caution.

In Fig. 6 we show our "experimental" optical potential as obtained by the procedure described above. In Figs. 6(a) and 6(b), the real and imaginary parts of the optical potential are plotted, respectively. In Fig. 6(b), two additional potentials from Eqs. (16) and (17) are shown. For convenience, these potentials have been normalized to the same value as our experimental V_{PI} at an arbitrarily selected energy of 81 eV. We notice that the potential of Duke *et al.*[26] overestimates V_{PI} at small energies before the plasmon cutoff energy, and, on the other hand, $-V_{PI}$ is too small just above the cutoff energy. By shifting the

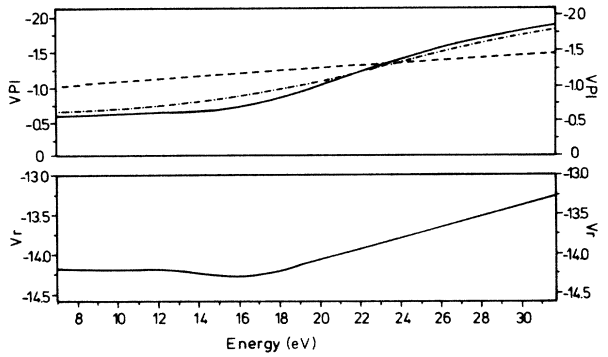

FIG. 6. The optical potential as a function of the electron energy: lower half, real part; upper part, imaginary part. The solid line is the result of this work, the dashed line is a modified result of Ref. 26 (see text), and the dashed-dotted line is the potential from Ref. 25.

potential of Andersson *et al.*[25] to correspond to ruthenium, i.e., by giving E_0 in Eq. (18) a value of 23 eV, we obtain the potential displayed in Fig. 6 as a dash-dotted line. This potential nearly coincides with our potential in the energy range studied here, giving a possible explanation of the origin of the potential of Andersson *et al.*;[25] i.e., Eq. (18) is some analytical approximation to the shape of the Hedin-Lundqvist potential. V_r in Eq. (20) is a relatively smooth function of energy having an average value of -8 eV. Michalk *et al.*[24] in their ordinary LEED study have obtained -14 eV for V_r. This difference of -6 eV could tentatively be explained by surface dipole contributions.[38]

E. Influence of the *z*-dependent surface barrier

To find out the effect of the *z*-dependent image-potential-type surface barrier we have carried out a set of calculations using the surface barrier as described in Eqs. (13) and (14), using the theory proposed in Eqs. (10) and (11). In Fig. 7 we compare spectra in which curves *a* and *c* are obtained using a step function for the surface barrier, whereas curves *b* and *d* are calculated using an image-potential-type surface barrier. Curves *c* and *d* were obtained taking V_{PI} constant and equal to -0.625 eV, and curves *a* and *b* were produced using the energy-dependent V_{PI}. As can be seen, no large changes occur for the minima around 11 eV. However, the spectra with image barrier fit the experimental results at low energies better, since the first minimum at 11.1 eV is now deeper than the 12.3-eV minimum. In Figs. 7(b) and 7(d), which are calculated with $\theta=3°$ towards ΓM, we get additional peaks due to image states. The exact energy positions of these image-potential-type surface-barrier-induced surface states depend on the selection of the parameters in Eqs. (14) and (15). The signal-to-noise ratio of our experimental equipment—though on a 2% level—does not allow the detection of these structures; even their theoretical intensities seem to be very small, except for the structures around 22 eV. The inclusion of the image-potential-type surface barrier (curve *d*) seems to overestimate spectral features by introducing strong spectral variations. The

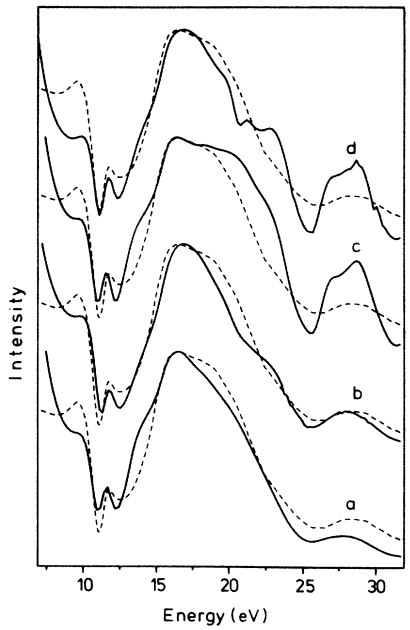

FIG. 7. Theoretical $I_{00}(E)$ calculated with varying $V_{PI}(E)$ (curves *a* and *b*) and with steplike or image-potential-like surface barrier (curves *b* and *d*). Dashed line displays the experimental spectrum.

use of the energy-dependent V_{PI} (curve *b*), however, improves the agreement in the 22-eV region by attenuation of the structures induced by the image potential.

It is worth mentioning that from our calculations with $|V_{PI}| < 0.054$ eV, we would derive a second image state to exist in our energy gap between 11 and 12 eV. This state, however, disappears with higher V_{PI} as shown in Fig. 8. With higher absolute values of V_{PI}, *IV* curves are identical to the *IV* curves in Fig. 3. We conclude that the theoretical condition for electrons to be in this state is a very long lifetime (V_{PI} small), but under the experimental conditions the lifetime is much shorter. As these two conditions are not fulfilled at the same time, we do not see

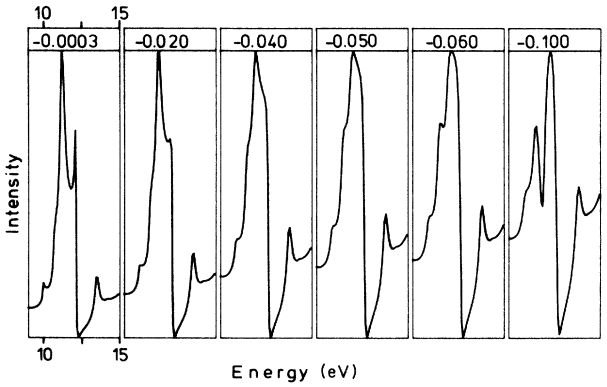

FIG. 8. Theoretical $I_{00}(E)$ calculated with image-potential-type surface barrier and small constant V_{PI}, showing the surface state at 11 eV with these small V_{PI}'s.

this peak in the spectra corresponding to the experimental situation. We can interpret this state as due to the image-potential-type surface barrier, since the state is absent with a step-function-type surface barrier, as can be seen in Fig. 3.

F. Influence of the ordinary LEED parameters

In ordinary LEED investigations, relaxations of the surface atom layer are important. Michalk *et al.*[24] have found, in their LEED study of Ru(001), that for the clean surface a contraction in the first-layer spacing, Δd_z, of $2\%\pm2\%$ occurs. In Fig. 9 we show the effect of variations of d_z on our spectra. As can be seen, there is a general shift of the spectral features to higher energies at a rate of 0.2 eV per 1% contraction. Furthermore, the relative intensities are strongly changed but the best agreement, as judged by eye, is obtained with 0% or 2% contraction. The intensity variation of the 28-eV structure complicates the determination of parameter c in Eq. (23) and we have obtained our c equal to 0.5 with $\Delta d_z=0\%$. We should stress that this conclusion would not be changed by a different choice of nonstructural parameters.

A second typical LEED parameter which we varied, was the average value of the real part of the optical potential with steplike surface barrier. It was found that the shape and energy positions of the minima around 11 eV are independent of this parameter. For an image-potential-type surface barrier this parameter, V_{r0} in Eq. (14), is much more important, since it dictates the energy positions of the wiggles due to image surface states (by changing the emerging energies of nonspecular beams). Furthermore, the behavior of the spectral features as a function of the polar angle of electrons depends on the value of this parameter. Since our experimental spectra do not show any detailed structures due to an image-potential-type surface barrier, we have not studied the influences of the other parameters in Eqs. (14) and (15) in more detail.

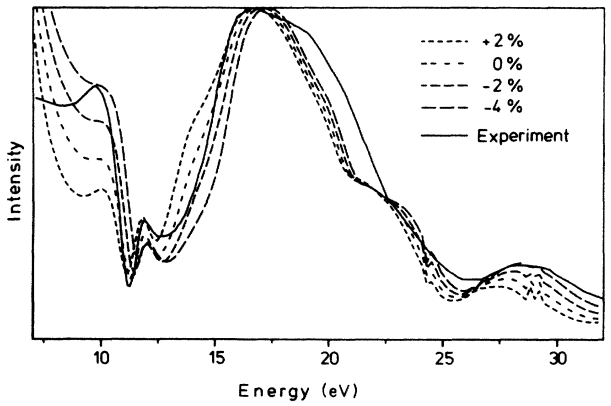

FIG. 9. Comparison of experimental $I_{00}(e)$ curve with theoretical curves obtained with varying distance between the first and the second atomic layers.

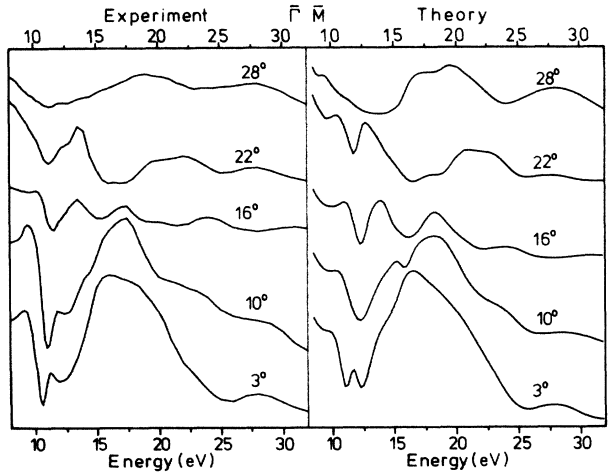

FIG. 10. Comparison of experimental and theoretical I_{00} curves for different polar angles towards $\bar{\Gamma}\bar{M}$. Calculational parameters are the same as in Fig. 5.

G. Off-normal *IV* curves

One crucial test of our theoretical model with energy-dependent V_{PI} is the angle dependence of the experimental and theoretical spectra. In Figs. 10 and 11 we show a set of experimental and theoretical spectra along $\bar{\Gamma}\bar{M}$ and $\bar{\Gamma}\bar{K}$, respectively. In Fig. 10 we have taken into account in our calculations both domains present in this $\mathbf{k}_{||}$ direction. The general agreement between theory and experiment is satisfactory. We have the same spectral structures present in both theoretical and experimental spectra. Also, the behavior of the intensity of the peaks in the spectra as a function of incidence angle is similar. This general agreement between theoretical and experimental spectra rules out the possibility that our good agreement near normal emission is accidental.

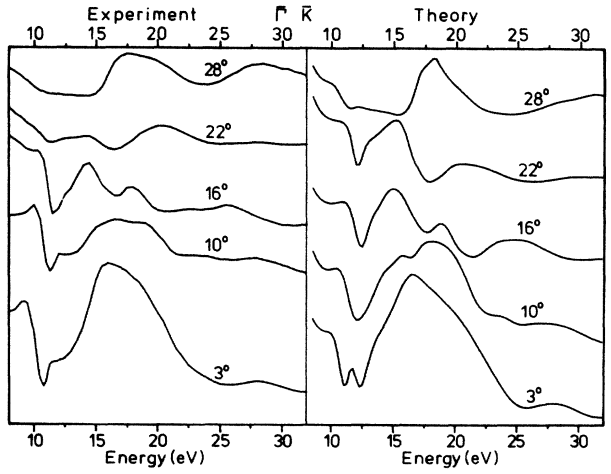

FIG. 11. Comparison of experimental and theoretical I_{00} curves for different polar angles towards $\bar{\Gamma}\bar{K}$. Calculational parameters are the same as in Fig. 5.

VI. CONCLUSIONS

Experimental results for the energy- and angle-dependent reflection coefficient for very-low-energy electrons in Ru(001) are presented, which show strong minima where peaks are observed in secondary-electron emission. A theoretical model is developed to trace these structures back to the unoccupied band structure. Calculations based on this model can describe the VLEED spectra very well.

(1) A necessary condition for successful calculations is an energy-dependent imaginary part of the optical potential with small absolute values for very low energies and increased value above the plasmon cutoff energy.

(2) The first strong reflection minimum (at 11.1 eV) is attributed to an unoccupied surface state and the second one (at 12.3 eV) to the high density of states in the *bulk* band structure, which couple well to free-electron-like states.

(3) There are some clear band-structure-induced spectral features, maxima and *minima*. However, direct assignments of extrema in the VLEED *IV* curves to symmetry points in the band structure without detailed calculations can be grossly wrong, because VLEED intensities are strongly influenced by other effects.

(4) The intensity of these spectral features depends on the coupling to free-electron-like bands.

(5) Some surface-state-induced structures might further obscure derivation of critical points.

ACKNOWLEDGMENTS

One of us (M.L.) is grateful to the Alexander von Humboldt Foundation (Bonn, Germany) for partial support. This work has been supported by the Deutsche Forschungsgemeinschaft (Bonn, Germany) through Sonderforschungsbereich 128.

---

*Permanent address: Department of Physics, Tampere University of Technology, P.O. Box 527, SF-33101 Tampere, Finland.

[1]G. Borstel, Appl. Phys. A **38**, 193 (1985).
[2]R. Feder, B. Awe, and E. Tamura, Surf. Sci. **157**, 183 (1985).
[3]R. C. Jaklevic and L. C. Davis, Phys. Rev. B **26**, 5391 (1982).
[4](a) F. J. Himpsel, K. Christmann, P. Heimann, and D. E. Eastman, Phys. Rev. B **23**, 2548 (1981); (b) P. Hofmann and D. Menzel, Surf. Sci. **152/3**, 382 (1985); (c) R. Hesse, P. Staib, and D. Menzel, Appl. Phys. **18**, 227 (1979).
[5]M. Lindroos, P. Hofmann, and D. Menzel, Phys. Rev. B **33**, 6798 (1986).
[6]L. R. Bedell and H. E. Farnsworth, Surf. Sci. **41**, 165 (1973).
[7]E. G. McRae and C. W. Caldwell, Surf. Sci. **57**, 63 (1976).
[8]S. A. Lindgren, L. Walldén, J. Rundgren, and P. Westrin, Phys. Rev. B **29**, 576 (1984).
[9]J. C. Le Bosse and J. Lopez, Surf. Sci. **162**, 953 (1985).
[10]L. Hedin and B. I. Lundqvist, J. Phys. C **4**, 2064 (1971).
[11]T. E. Madey and D. Menzel, Jpn. J. Appl. Phys., Suppl. 2, part 2, 229 (1974).
[12]P. Feulner and D. Menzel, Surf. Sci. **154**, 465 (1985).
[13]M. Lindroos, H. Pfnür, P. Hofmann, and D. Menzel (unpublished).
[14]J. B. Pendry, Surf. Sci. **57**, 679 (1976).
[15]I. Adawi, Phys. Rev. **134**, A788 (1964).
[16]J. F. L. Hopkinson, J. B. Pendry, and D. J. Titterington, Comput. Phys. Commun. **19**, 69 (1980).
[17]J. B. Pendry, *Low Energy Electron Diffraction* (Academic, London, 1974).
[18]M. A. Van Hove and S. Y. Tong, *Surface Crystallography by LEED* (Springer-Verlag, Berlin, 1979).
[19]C. G. Larsson, Surf. Sci. **152/3**, 213 (1985).
[20]K. Kambe, Z. Naturforsch. **22**, 322 (1967); **22**, 422 (1967).
[21]J. L. Moruzzi, A. R. Williams, and J. F. Janak, *Calculated Electronic Properties of Metals* (Pergamon, New York, 1978).
[22]B. M. Hall and S. Y. Tong, J. Vac. Sci. Technol. **20**, 578 (1982).
[23]G. Malmström and J. Rundgren, Comput. Phys. Commun. **19**, 263 (1980); J. Rundgren and G. Malmström, J. Phys. C **10**, 4671 (1977).
[24]G. Michalk, W. Moritz, H. Pfnür, and D. Menzel, Surf. Sci. **129**, 92 (1983).
[25]S. Andersson, B. Kasemo, J. B. Pendry, and M. A. Van Hove, Phys. Rev. Lett. **31**, 595 (1973).
[26]C. B. Duke and C. W. Tucker, Jr., Phys. Rev. Lett. **23**, 1163 (1969).
[27]L. J. Clarke, *Surface Crystallography* (Wiley, New York, 1985).
[28]B. I. Lundqvist, Phys. Status Solidi **32**, 273 (1969).
[29]J. Neve, J. Rundgren, and P. Westrin, J. Phys. C **15**, 4391 (1982).
[30]J. J. Quinn, Phys. Rev. **126**, 1453 (1962).
[31]E. Umbach, Surf. Sci. **117**, 482 (1982).
[32]V. Heine, Proc. Phys. Soc. London **81**, 300 (1963).
[33]C. D. Mahan, Phys. Rev. B **2**, 4334 (1970).
[34]F. Forstmann and J. B. Pendry, Z. Phys. **235**, 75 (1970).
[35]M. Lindroos, H. Pfnür, and D. Menzel (unpublished).
[36]J. C. LeBosse, J. Lopez, C. Gaubert, Y. Cauthier, and R. Baudoing, J. Phys. C **15**, 6087 (1982); J. C. LeBosse, J. Lopez, C. Gaubert, Y. Cauthier, and R. Baudoing, *ibid.* **15**, 3425 (1982).
[37]J. B. Pendry and S. J. Gurman, Surf. Sci. **49**, 87 (1975).
[38]P. J. Jennings and S. M. Thurgate, Surf. Sci. **104**, 1210 (1981).